ELSEVIER

Cardiovascular Research 50 (2001) 301–313

Cardiovascular Research

www.elsevier.com/locate/cardiores
www.elsevier.nl/locate/cardiores

Cellular consequences of HERG mutations in the long QT syndrome: precursors to sudden cardiac death

Colleen E. Clancy, Yoram Rudy*

Cardiac Bioelectricity Research and Training Center, Department of Physiology and Biophysics, Department of Biomedical Engineering, 509 Wickenden Building, Case Western Reserve University, Cleveland, OH 44106-7207, USA

Received 1 September 2000; accepted 15 November 2000

Abstract

Background: A variety of mutations in HERG, the major subunit of the rapidly activating component of the cardiac delayed rectifier I_{Kr}, have been found to underlie the congenital Long-QT syndrome, LQT2. LQT2 may give rise to severe arrhythmogenic phenotypes leading to sudden cardiac death. **Objective:** We attempt to elucidate the mechanisms by which heterogeneous LQT2 genotypes can lead to prolongation of the action potential duration (APD) and consequently the QT interval on the ECG. **Methods:** We develop Markovian models of wild-type (WT) and mutant I_{Kr} channels and incorporate these models into a comprehensive model of the cardiac ventricular cell. **Results:** Using this virtual transgenic cell model, we describe the effects of HERG mutations on the cardiac ventricular action potential (AP) and provide insight into the mechanism by which each defect results in a net loss of repolarizing current and prolongation of APD. **Conclusions:** This study demonstrates which mutations can prolong APD sufficiently to generate early afterdepolarizations (EADs), which may trigger life-threatening arrhythmias. The severity of the phenotype is shown to depend on the specific kinetic changes and how they affect I_{Kr} during the time course of the action potential. Clarifying how defects in HERG can lead to impaired cellular electrophysiology can improve our understanding of the link between channel structure and cellular function.

Keywords: Arrhythmia (mechanisms); Computer modelling; K-channel; Long QT syndrome; Sudden death; Ventricular arrhythmias

1. Introduction

Increasingly, seemingly idiopathic syndromes are being linked to genetic defects. A recent example is the congenital Long-QT (LQT) syndrome [1–3]. The syndrome is associated with prolongation of the Q-T interval on the ECG, which may precede syncope and sudden cardiac death. In 1995, patients from a family afflicted with a genetically linked form of the Long-QT syndrome (LQT2) were found to have abnormalities in the HERG gene [4]. This gene underlies a potassium channel that is highly expressed in the heart with properties similar to the E-4031 sensitive current [5,6]. Many experiments have since demonstrated that HERG encodes the major subunit of the rapidly activating component of the cardiac delayed rectifier current (I_{Kr}). Very recently the minK-related peptide 1 (MiRP1) was shown to stably assemble with HERG and give rise to a current strikingly similar to native I_{Kr} [7].

We develop a structurally based model of cardiac I_{Kr} in order to elucidate the functional consequences of gene defects in cardiac HERG that lead to abnormalities in repolarization. We have drawn from a variety of experiments presented in the peer-reviewed literature in order to build a robust model that accounts for the breadth of published data. More than 50 mutations in HERG have been linked to the congenital Long-QT syndrome [3]. Defects in the HERG pore have been shown to have heterogeneous cellular phenotypes. Pore mutations may result in a loss of function, sometimes due to a trafficking defect [8], and may or may not coassemble with WT HERG subunits to exert dominant negative effects [9]. Other defects in the channel pore give rise to altered

*Corresponding author. Tel.: +1-216-368-4051; fax: +1-216-368-8672.

E-mail address: yxr@po.cwru.edu (Y. Rudy).

Time for primary review 27 days.

0008-6363/01/$ – see front matter
PII: S0008-6363(00)00293-5

channel kinetics leading to decreased repolarizing current [10,11]. Nearby mutations in the S4–S5 linker have been shown to variably affect activation [12].

Here, we use Markov models of wild-type (WT) and mutant I_{Kr} in a cardiac ventricular cell model to evaluate the cellular arrhythmogenic consequences of several HERG mutations associated with LQT2. The Markov models allow for the introduction of state-specific kinetic changes due to mutation induced structural defects. These changes affect adjacent channel states through coupling. We choose as examples two well-characterized defects that alter cell electrophysiology through their effects on channel kinetics. The first, the T474I point mutation, results in an altered voltage dependence of activation coupled with a reduction in macroscopic current density. The second, the R56Q mutation, is a point mutation in the Per–Arnt–Sim (PAS) domain located in the amino-terminus (N-terminus) region of HERG, which normally interacts with the channel and reduces the rate of deactivation [13]. Mutations in this region presumably prevent proper association of the N-terminus with the channel and act to increase the rate of channel deactivation. We choose these two defects as examples of mutations that exert their effects on cellular behavior by reducing the I_{Kr} repolarizing current through alterations in its channel kinetics.

We have also investigated the effects of the N629D mutation, a 'gain of function' defect in HERG that results in loss of C-type inactivation coupled with loss of K^+ selectivity [14]. HERG contains a pore selectivity sequence that is changed by the mutation from GFGN to GFGD, allowing for non-specific passage of monovalent cations. In this study, we incorporate these changes into our model of I_{Kr} and investigate the effects on the morphology of the action potential and action potential duration.

In addition, we elucidate the effects of a range of reduction in current on the action potential duration (APD), since many HERG defects exert their effects through a dominant negative mechanism, trafficking defects, or reduced mutant protein expression [3]. Finally we evaluate the electrophysiological consequences of a 'functional knockout' mutation, where I_{Kr} current is absent, a situation described clinically in a patient born with such a defect [15]. In all, we provide several examples of heterogeneous genotypes and the mechanism by which each prolongs APD leading to a prolonged QT interval in the ECG, increased dispersion of repolarization, and possibly the development of early afterdepolarizations (EADs) and cardiac arrhythmias.

2. Methods

The general approach to modeling the action potential (AP) is the same as that described for the dynamic Luo–Rudy (LRd) model of a ventricular cell [16] with modifications described in later publications [17,18]. The fast sodium current (I_{Na}) was recently reformulated using a Markovian approach and incorporated into the whole-cell model [19]. We use a similar approach to reformulate I_{Kr}. Macroscopic current density is given by:

$$I_s = G_s \cdot P_{O,s} \cdot (V_m - E_{rev}) \quad \text{where} \quad G_s = \sigma \cdot g_s \tag{1}$$

$P_{O,s}$ is the sum of all channel open probabilities, V_m is the membrane potential, and E_{rev} is the reversal potential. G_s is the maximum membrane conductance (channel density (σ) times the unitary channel conductance (g_s)). The channel state probabilities are described by first order differential equations using the methods described in [20]. The model parameters are fit using averaged measured activation, inactivation and deactivation data [5,6,21–23]. Parameters are then optimized to account for the proper behavior of macroscopic currents compared to data recorded at physiological temperatures and ion concentrations from guinea pig ventricular myocytes (see Figs. 3 and 4).

All the simulations were encoded in C/C++. Simulations were implemented (double precision) on a Sun Workstation Ultra 1. A time step of 0.005 ms was used during the stimulus and AP upstroke. At all other times, a 0.01-ms time step was used.

The model for cardiac I_{Kr} is shown in Fig. 1. The model includes three closed states (C3, C2, C1), an open state (O), and an inactivation state (I). The transition between C2 and C1 is voltage independent [21]. Closed state inactivation (C1→I) is included from a single closed state, allowing for reduced computation time. The transition rate between C1 and I is the same as from C1 to O [24]. I_{Kr} exhibits strong inward rectification due to a rapid voltage dependent C-type inactivation at positive membrane potentials [11] (transition from O to I). The transitions between O and I are also dependent on extracellular potassium concentration $[K^+]_{out}$ [25]. As $[K^+]_{out}$ is increased the transition rates decrease. In addition, the maximum conductance of I_{Kr} (G_{Kr}) depends on $[K^+]_{out}$. These dependences on $[K^+]_{out}$ are introduced into the model.

Action potential simulations are carried out in epicardial and midmyocardial (M) cells. Epicardial and M cells are simulated by varying the membrane conductance of I_{Ks} (G_{Ks}) as described previously [18]. Equations of the LRd model can be found in previous publications [16,17,26,27] and can be downloaded from the research section of http://www.cwru.edu/med/CBRTC

3. Results

3.1. Simulated wild type (WT) behavior

The overall result of decreased rates of inactivation and recovery from inactivation at high $[K^+]_{out}$ is an inactiva-

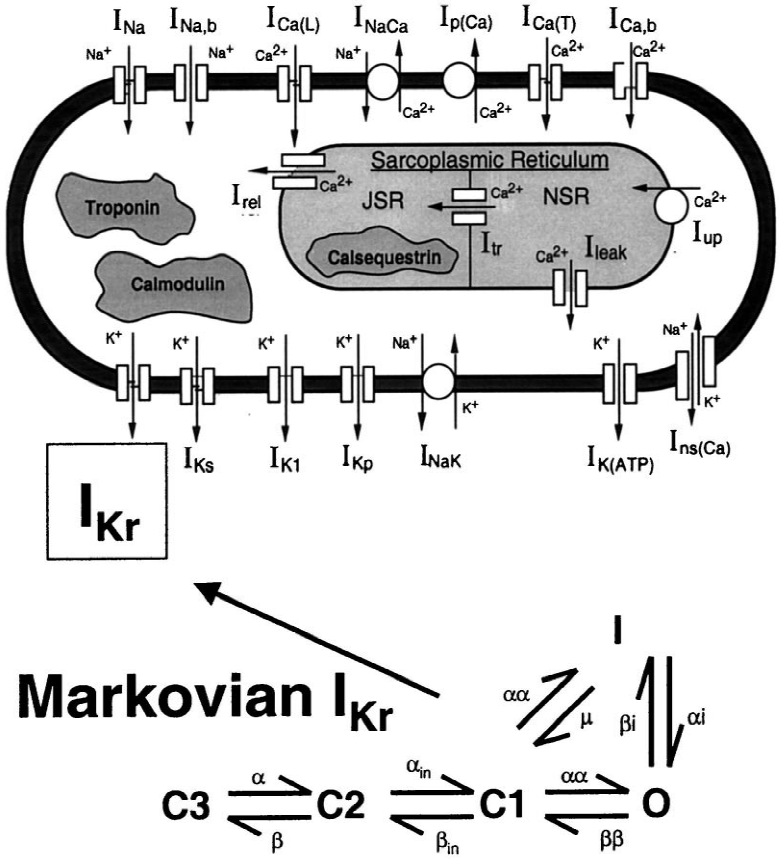

Fig. 1. Markovian model of cardiac I_{Kr} introduced into the Luo–Rudy dynamic (LRd) model of the cardiac ventricular cell [16]. Details of the cell model are provided in Refs. [16–18,27].

tion state that is more absorbing. This is demonstrated in the single channel gating of I_{Kr} in Fig. 2 (left panels) and channel mean open times (MOTs) (right panels). Panel A (left) shows experimentally recorded single channel gating of HERG channels at 21°C and 100 mM $[K^+]_{out}$ [24]. Single channels are depolarized from a holding potential of −80 to 100 mV for 300 ms and subsequently hyperpolarized (arrow) to −120 mV for 100 ms (inset, bottom of Fig. 2). Experimental unitary HERG currents (panel A, left) are compared to simulated single channel gating of I_{Kr} (panel B, left) at 100 mM $[K^+]_{out}$ [24]. The simulated single channel gating is at 37°C. The single channel gating behavior in the experiments and the simulations demonstrates channel inactivation from closed states and recovery from inactivation through the open state. Channels may fail to open during depolarization (single channel traces before arrow), due to inactivation from closed states, but conduct an inward current during subsequent hyperpolarization (traces after arrow) due to recovery from channel inactivation through the open state. The experimental traces show a longer latency to first opening compared to the simulations, an expected behavior at the lower temperature under which the experiments are conducted. The model predicts gating behavior at physiological $[K^+]_{out}$ of 4.5 mM in panel C. Here, the inactivation state is less absorbing compared to panels A and B, an overall result of increased rates of inactivation and recovery from inactivation at lower $[K^+]_{out}$. Hence, more channel openings are observed during the depolarization step and the subsequent hyperpolarization (panel C, left). This behavior is consistent with macroscopic current recordings at physiological $[K^+]_{out}$, which have a persistent component of outward current during depolarization (see Fig. 4: experiment, top traces; simulation, bottom traces). This persistent current rapidly reaches a pseudo-steady state due to the rapid equilibrium between open and inactivation states. The MOTs of experimentally recorded HERG channels at $[K^+]_{out}=100$ mM [24] (panel A, right) and simulated I_{Kr} channels at $[K^+]_{out}=100$ mM and $[K^+]_{out}=4.5$ mM (right panels B and C, respectively) are shown for comparison. The simulated MOTs are computed as 1/(sum of transition rates leaving the open state, $\beta\beta+\beta i$). At physiological $[K^+]_{out}=4.5$ mM, MOTs are shorter due to the increased inactivation rate. This comparison demonstrates that both the simulated and experimentally obtained MOTs exhibit weak voltage dependence over a wide range of voltage regardless of $[K^+]_{out}$ [6,24].

The voltage dependence of activation and rectification (inactivation) of macroscopic I_{Kr} is shown in Fig. 3. The activation curve (panel A) is constructed by normalizing

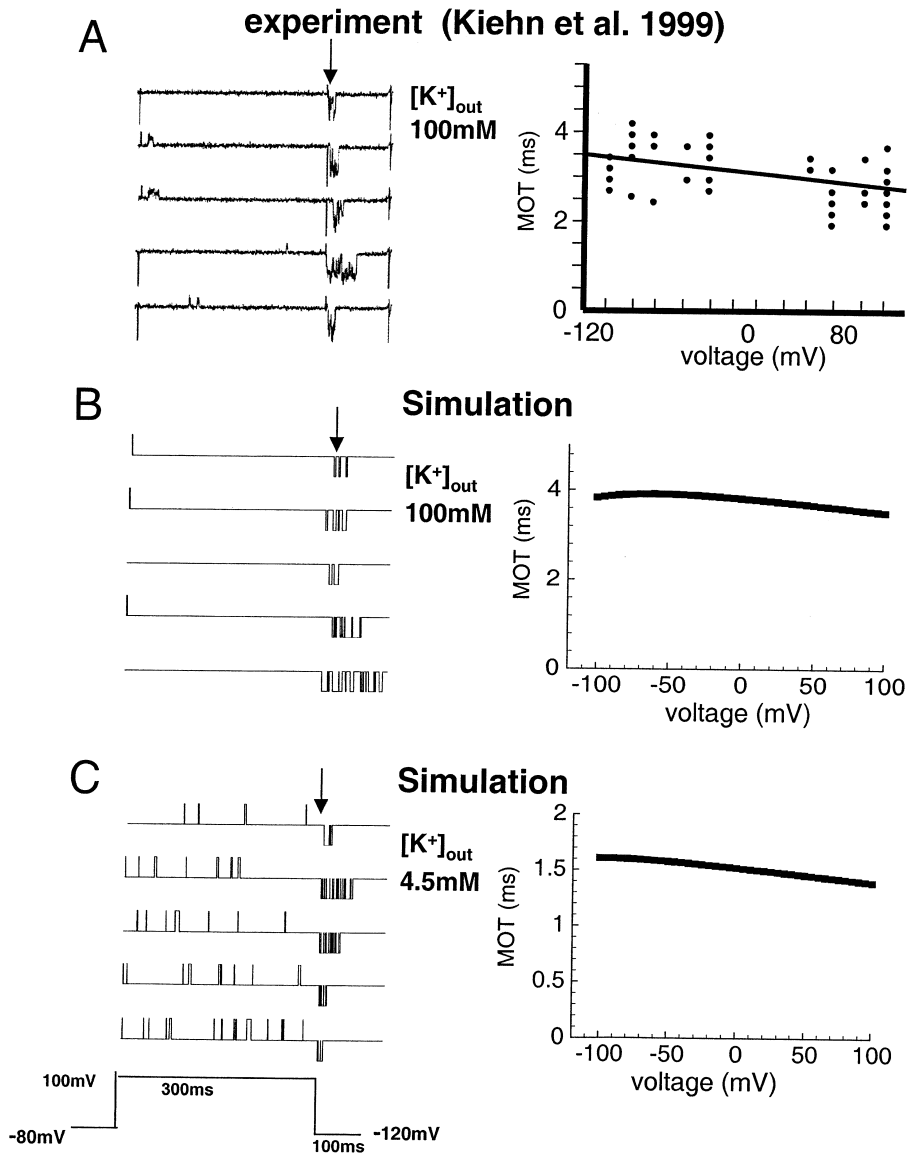

Fig. 2. Simulated single channel gating of model I_{Kr} (left, panels B and C) is compared to experimentally measured single channel gating of HERG at 100 mM $[K^+]_{out}$ (panel A, left) [24]. Simulations are conducted at 100 mM $[K^+]_{out}$ (panel B) and physiological 4.5 mM $[K^+]_{out}$ (panel C). The mean open times MOT of experimentally recorded HERG and simulated I_{Kr} are shown on the right. Panels A (experiment) and B (simulation) are MOTs at 100 mM $[K^+]_{out}$. Panel C (right) shows simulated MOTs at physiological $[K^+]_{out}=4.5$ mM.

peak tail current at the indicated test potential to the maximum tail current during repolarization (−100 mV). The solid line is the simulation; filled boxes are experimental data obtained from the E-4031 sensitive current in guinea pig ventricular myocytes [5]. The rectification (R) curve (panel B) is computed as:

$R = (\text{peak } I_{Kr})/(\text{peak } I_{Kr} \text{ in the absence of rectification})$

Computation of the rectification (inactivation) curve using this method more accurately describes channel inactivation than a standard inactivation protocol since I_{Kr} availability can be contaminated by deactivation at membrane potentials below 0 mV [7,11]. Rectification is removed in the simulation by making the O→I transition rate equal to zero. The simulated rectification curve is compared to experimental data from Sanguinetti and Jurkiewicz (filled circles) [5]. Rectification is obtained experimentally by extrapolating the linear portion of the peak tail current I–V curve into the positive potential range [5].

G_{Kr} is affected by variations in $[K^+]_{out}$. In Fig. 3C, the peak tail current–voltage relationship is shown for $[K^+]_{in}=150$ mM and $[K^+]_{out}=5.4$, 50 and 150 mM. Simulated I–V curves (top) are compared to experimentally recorded rabbit I_{Kr} (bottom) using the same protocol as in Shibasaki [6]. From a holding potential of −43 mV, the cell is pulsed to the test potential for 500 ms. A subsequent pulse to −43 mV for $[K^+]_{out}=5.4$, and −73 mV for

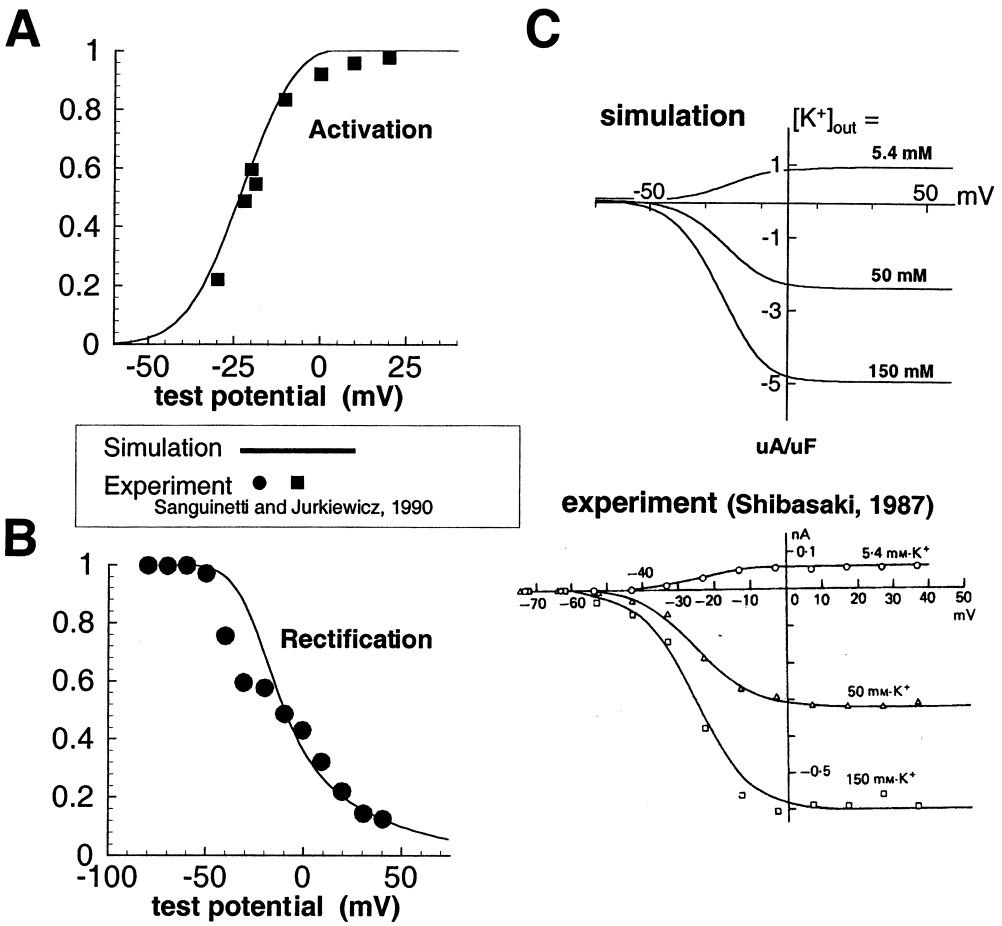

Fig. 3. Activation (A) and rectification (B) curves are constructed from model I_{Kr} and compared to experimentally recorded guinea pig I_{Kr} at physiological temperature and ion concentrations [5]. The simulated current–voltage (I–V) relationship at three different $[K^+]_{out}$ is shown (C, top) and compared to experimental data (C, bottom) from Shibasaki [6]. See text for protocol.

$[K^+]_{out}=50$ and 150 mM elicits a tail current that is plotted as a function of the test potential. Notice that at $[K^+]_{out}=5.4$ mM, the tail current is outward at all membrane potentials ($E_{rev}=-89$ mV) and exhibits strong inward rectification at positive potentials that compares well with the degree of rectification seen experimentally. At $[K^+]_{out}=50$ mM and $[K^+]_{out}=150$ mM, the tail current is inward in both the simulation and the experiment due to the equilibrium potentials of -29 and 0 mV at 50 and 150 mM $[K^+]_{out}$, respectively.

Fig. 4 (panel A) contains experimentally recorded I_{Kr} current traces from guinea pig ventricular myocytes [5]. Cells are depolarized for 250 ms from a holding potential of -40 mV and are subsequently repolarized to -40 mV for 750 ms (see protocol, inset). Simulated currents following the same protocol are shown in panel B. The tail current is plotted on a reduced time scale in order to be consistent with the experimental traces [5]. At a test potential of 10 mV or greater, hyperpolarization elicits an outward tail current hook experimentally and in the simulation (arrow). This hook is absent at test potentials 0 mV (arrow) or smaller. The hook reflects recovery from inactivation through the open state. Since recovery from inactivation (I→O) is very fast compared to deactivation (O→C1), a large outward tail current is conducted as channels slowly return to the closed resting states.

3.2. Simulated HERG mutations

The T474I mutation, a point mutation in the S2–S3 linker, alters gating properties and reduces macroscopic I_{Kr} [28,29]. We simulate these changes by altering the voltage dependence of the activation transition rates (α and $\alpha\alpha$, see Fig. 1 and Appendix) and reducing G_{Kr} by 35%. Fig. 5 compares simulated (panel B) activation and I–V curves for WT and T474I mutant I_{Kr} to experimentally measured (panel A) curves. The activation curves (protocol described for Fig. 3) are shown in the left panels. The experimentally measured $V_{1/2}$ for WT and T474I is -15.9 and -43.2 mV, respectively (a shift of -27.3 mV for T474I relative to WT) [28]. The T474I simulated activation curve is shifted by -24 mV ($V_{1/2}=-47$ mV) relative to the WT curve ($V_{1/2}=-23$ mV). Experimental recordings were performed at 22–23°C, while the simulations were performed at

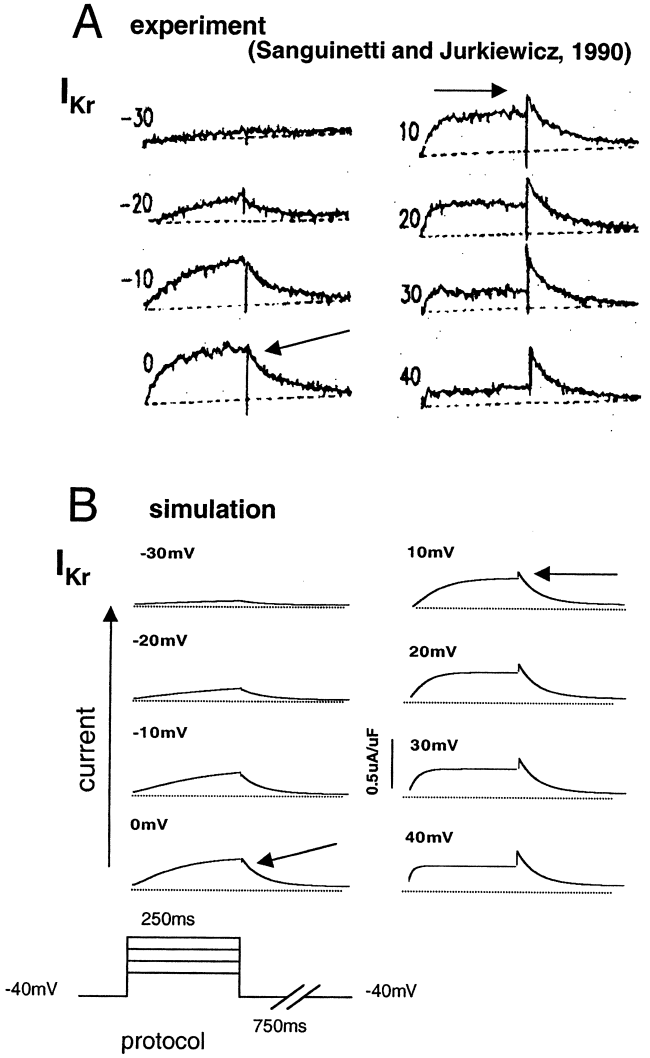

Fig. 4. Time course of model I_{Kr} compared to experimentally recorded I_{Kr} at physiological temperature and ion concentrations [5]. The cell is depolarized to the indicated test potential for 250 ms from a holding potential of −40 mV and then repolarized to −40 mV (inset).

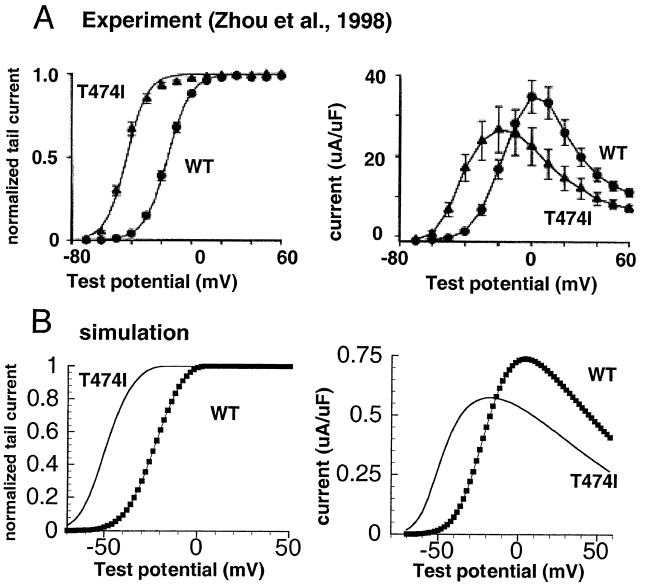

Fig. 5. The T474I mutation affects the voltage dependence of activation. Activation curves are shown for experimental (A, left) and simulated (B, left) WT and T474I mutants. The fully activated *I–V* relationship (steady-state current) is shown for experimental (A, right) and simulated (B, right) WT and T474I mutant channels.

physiological temperature (37°C). The leftward shift of the simulated activation curves relative to measured curves is an expected result of the increased temperature [22]. The fully activated *I–V* relationships of simulated I_{Kr} and experimentally recorded HERG are shown in the right panels of Fig. 5 (protocol described in Zhou et al. [28]). The mutant peak tail current is shifted by −20 mV relative to WT in the experimentally recorded and simulated curves. The maximum mutant current is 65% of WT levels.

Mutations in the PAS domain of the amino terminal of HERG act to increase the rate of deactivation [30]. We focus on the R56Q mutation since this mutant can increase the rate of deactivation most profoundly [30]. The mutation is simulated by increasing the O→C1 transition rate by a factor of 6.3 and the C2→C3 rate by a factor of 10.5 [30]. These increased rates of deactivation result in a rightward shift in the voltage dependence of activation and rectification (not shown), due to the strong coupling between the discrete states. The simulated kinetic changes result in shifts of +18 mV in the activation curve and +16 mV in the rectification curve. These shifts are also seen experimentally in HERG channels containing the R56Q mutation expressed in *Xenopus* oocytes [30] (not shown).

Fig. 6 compares action potentials from WT, T474I and R56Q simulated M-cells. The 1000th AP is shown at a cycle length (CL) of 750 ms. The left panel illustrates a WT M-cell action potential (AP). The AP duration at 90% repolarization (APD_{90}) is 164 ms. The corresponding I_{Kr} current during the AP is shown in panel B. Channel state probabilities during the AP are shown in panels C through G (see model in Fig. 1). During the AP upstroke, channels move from the leftmost closed state (C3, panel C) and pass through C2 and C1 (panels D and E, respectively). From the C1 state, channels can pass directly to the open state (O, panel F) or to an unavailable inactivation state I (panel G). Once the channels open, they rapidly inactivate (transition from O→ I). A pseudo-equilibrium is reached between the inactivation transition (O→I) and recovery from inactivation (I→O) that begins to favor recovery as the AP plateau repolarizes. As recovery from inactivation becomes more likely, I_{Kr} increases to a pronounced peak (arrow) and contributes to the faster repolarization late in the AP. At this time channels slowly deactivate (O→C1 transition).

In Fig. 6, the middle panel shows I_{Kr} and associated channel state probabilities during the AP for a T474I mutant M-cell (compare to WT). In addition to the kinetic

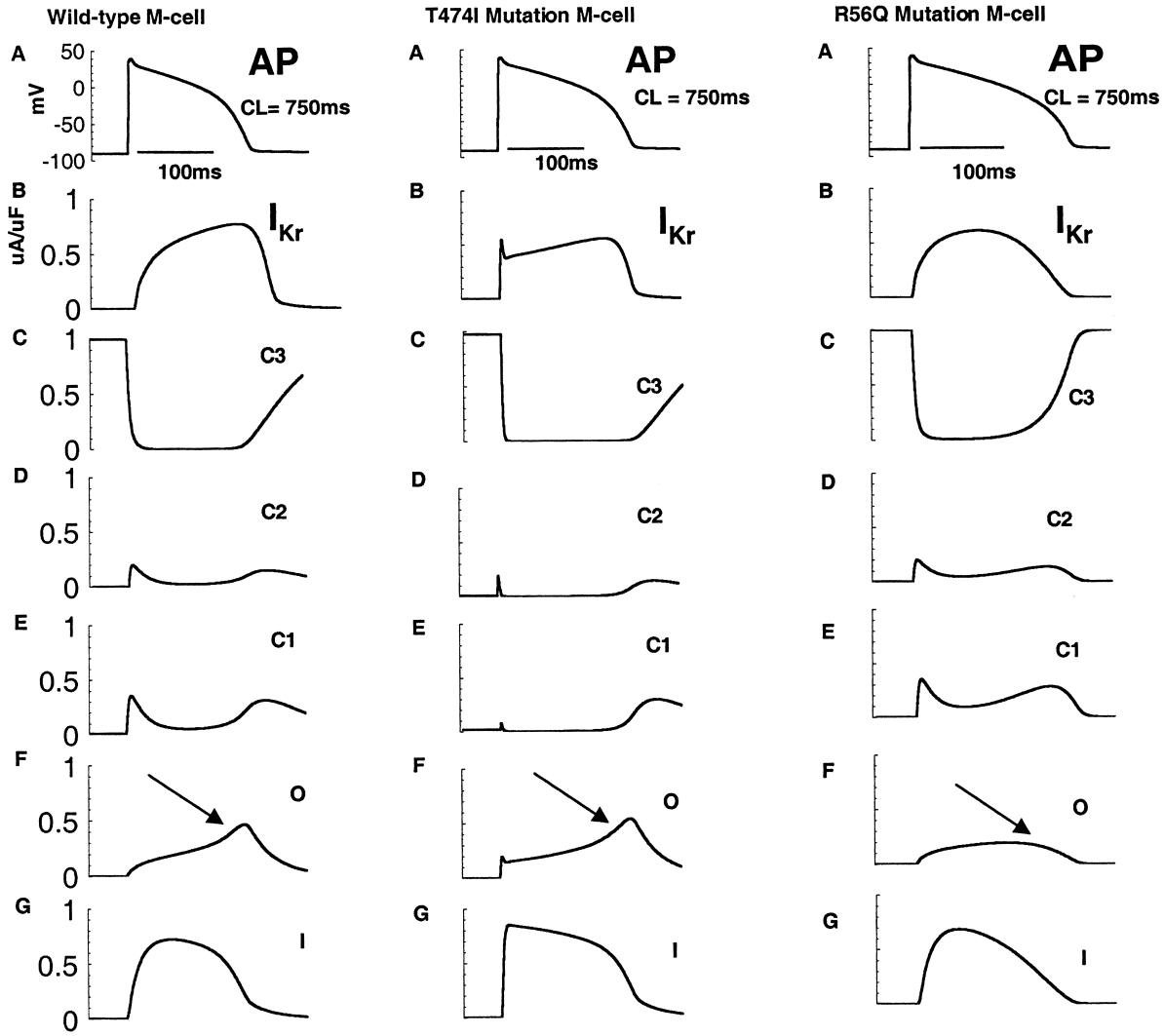

Fig. 6. Action potential (AP) of 1000th paced beat of a wild-type (WT) M-cell paced at a cycle length (CL)=750 ms, is shown in panel A, left. Panel B is the corresponding I_{Kr} during the AP. Panels C–G are the probabilities of residence in the indicated states over the course of the AP (see Fig. 1 for the definition of channel states). The 1000th paced beat of a T474I affected M-cell is shown in the middle panel. Effects of the R56Q mutation on the AP are shown on the right.

changes, G_{Kr} is reduced by 35% in the simulation. Mutant APD is 16 ms longer than WT. Interestingly, the reduction in G_{Kr}, rather than altered channel kinetics, is the major factor in lengthening APD. The alterations in activation kinetics alone have only a minor effect on APD (not shown). The morphology of I_{Kr} early in the AP is altered due to the shift in the voltage dependence of activation. The leftward shift of the activation curve results in early channel openings at less depolarized membrane potentials (panel F, compare to WT, panel F) and an increased rate of I_{Kr} activation (panel B). Channels in the open state are available to inactivate earlier (panel G), resulting in the large notch following activation at the beginning of the current trace (panel B) which reflects fast inactivation. The channel open probability late in the AP (panel F), when I_{Kr} plays a major role in repolarization, displays a pronounced peak (arrow) and is similar to that of WT I_{Kr}.

The effect of the R56Q mutation on the cardiac AP is shown in an M-cell in the right panel of Fig. 6. While initial I_{Kr} elicited during the upstroke of the AP is comparable between the WT and R56Q mutant cells (panel B, compare to WT), the late current in the mutant is decreased due to increased probability of the O→C1 transition. This is seen in the open probability during the AP, shown in panel F. In contrast to WT and T474I mutant currents, the R56Q mutant lacks a peak in P(O) late in the AP (panel F, arrow). Deactivation occurs earlier, resulting in less repolarizing current late in the AP where I_{Kr} usually plays a major role in repolarization and determining APD.

Fig. 7 shows the rate dependence of APD in WT (panel A) and the two kinetic mutants T474I (panel B) and R56Q (panel C). There is only a slight prolongation at slow rate in mutant epicardial cells compared to WT (top). However, mutant M cells show significantly greater APD prolonga-

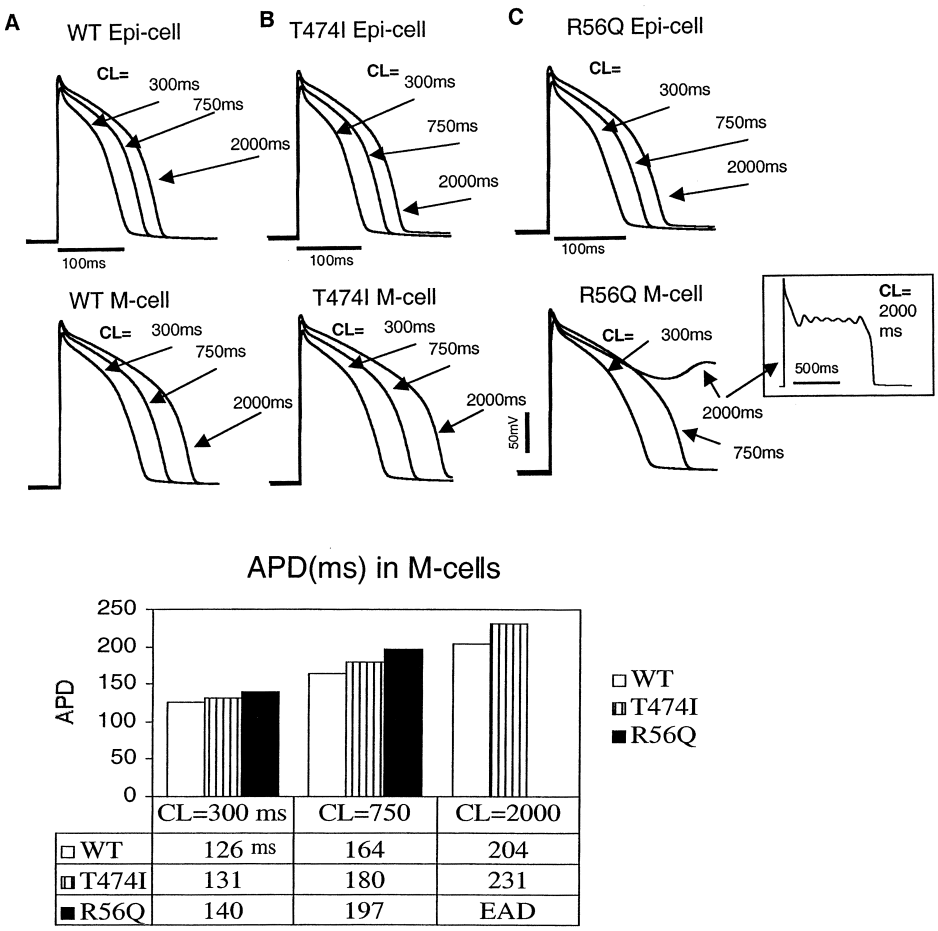

	CL=300 ms	CL=750	CL=2000
□ WT	126 ms	164	204
◧ T474I	131	180	231
■ R56Q	140	197	EAD

Fig. 7. Rate dependence of APD in WT (A), T474I (B), and R56Q (C) cells. Epicardial cells are shown in the top panels, M-cells in the bottom. M-cells APD is preferentially prolonged at slow rate for both mutations. The table summarizes the rate dependence of APD in M-cells. Values for APD are given in the bottom for each mutant at the different CL.

tion with decreasing rate (Fig. 7, bottom and table). The R56Q mutation gives rise to a prolonged APD which develops EADs (panel C, bottom inset) at CL = 2000 ms (bradycardia).

Fig. 8 demonstrates the effects of the N629D gain of function mutation on the action potential in epicardial (panel A) and M-cells (panels C and E). All cells are paced at a CL = 1000 ms for 1000 beats. The corresponding I_{Kr} is shown beneath each AP trace (panels B, D and F). The mutation is characterized by a loss of C-type inactivation and of ion selectivity, allowing for the passage of Na^+ ions in addition to K^+ ions. The relative selectivity of the channel for Na^+ and K^+ (P_{Na}/P_K) is 0.65 [14]. We simulate the mutation by eliminating C-type inactivation (O→I transition rate = 0) and by altering selectivity to the ratio above. Using the Nernst equation, we compute the reversal potential of the N629D I_{Kr} to be −13 mV. This reversal potential for mutant I_{Kr} falls within the range of physiological plateau potentials. As a result, early I_{Kr} is an outward repolarizing current carried by K^+. However, when the membrane potential repolarizes below −13 mV, the current is inward and carried by Na^+. This is demonstrated in the I_{Kr} traces during epicardial APs shown in Fig. 8, panel B. During the initial phase of the action potential I_{Kr} is outward, but once the repolarizing membrane potential passes the reversal potential threshold, the current becomes inward (arrows). The inward current late in the plateau results in severe APD prolongation. Even more severe, are the effects of this mutation in M-cells (panel C and E). In panel C, we show an M-cell with G_{Ks}:G_{Kr} = 7:1, and in panel E an M-cell with G_{Ks}:G_{Kr} = 12:1, both of which fall within the physiological range for currents measured in M-cells. In both M-cells, the inward I_{Kr} carried by Na^+ on the background of the smaller I_{Ks} of M-cells, acts to sufficiently prolong the AP plateau to allow for L-type Ca^{2+} channels recovery and reactivation resulting in EADs [26,31]. The morphology of the AP is profoundly disrupted as a result of this mutation.

Fig. 9 demonstrates the effects on the AP of HERG mutations resulting in decreased density of functional channels. We simulate the effect of the resulting current suppression on the morphology and duration of the AP in M-cells. In epicardial cells, these reductions act to prolong APD but do not give rise to the development of EADs (not

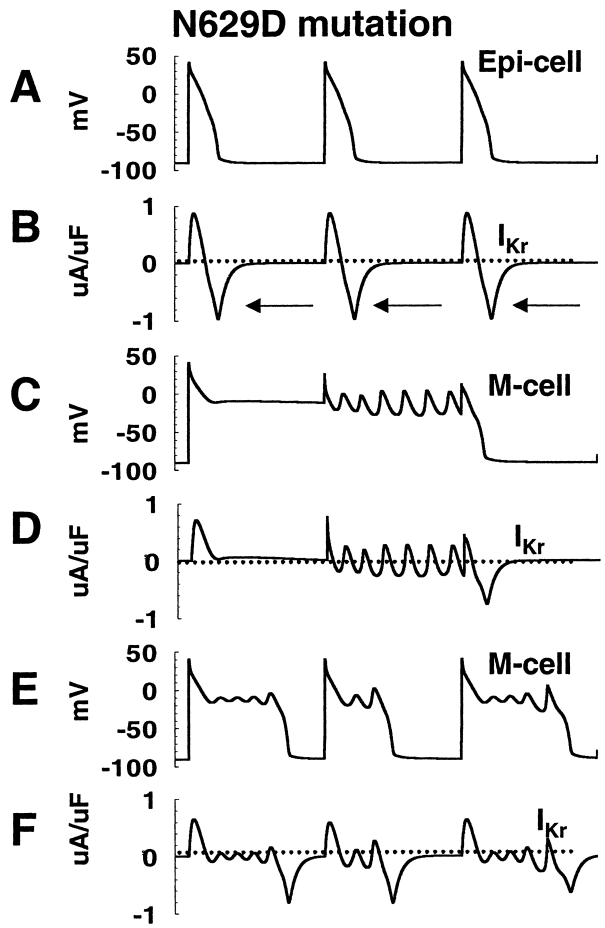

Fig. 8. The N629D mutation effects on the action potential and macroscopic I_{Kr}. In panel A, an epicardial cell paced for 1000 beats at a cycle length of 1000 ms is shown. The corresponding I_{Kr} is shown in B. The mutation results in removal of C-type inactivation and renders the channel pore non-selective among cations. The inward current (arrows, panel B) is carried by Na^+ and acts to disrupt the delicate balance of currents during the plateau, shifting it in the inward (depolarizing) direction. Two species of M-cells are shown in panels C (G_{Ks}:G_{Kr}=7:1) and E (G_{Ks}:G_{Kr}=12:1) with corresponding I_{Kr} shown in D and F, respectively. The mutation profoundly affects the AP morphology in M-cells and leads to EAD formation.

shown). We consider 25, 50 and 75% reductions as corresponding to defects due to defective protein expression [32], impaired transport to the cell surface [28], or dominant negative suppression [9], respectively. A simulation showing the effects of reduced macroscopic current has been conducted previously in a Hodgkin–Huxely model of I_{Kr} [33]. Here we investigate the effects of a range of current reduction using the Markov I_{Kr} model in M-cells. APDs of the mutant M-cells are markedly affected over the range of reductions tested (Fig. 9). For a 75% reduction at slow rates (CL=1000 ms) the AP is marked by EADs (Fig. 9, arrow).

Fig. 10 (panels A and B) demonstrates the effects of changes in pacing rate in a cell with a 50% loss of functional I_{Kr} channels. In epicardial cells (panel A) the resulting reduction in current gives rise to a subtle

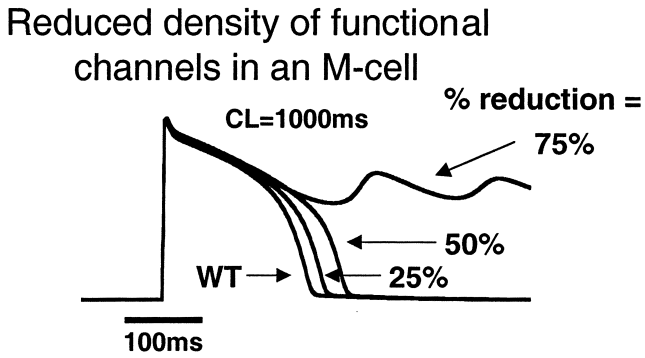

Fig. 9. Variable loss of functioning channels can arise from different mutations. Here the effects of a 25, 50 and 75% loss on APD in an M-cell is shown after 1000 paced beats at a CL=1000 ms. A 25% loss may arise from a reduction in mutant protein expression. The 50 and 75% losses may result from trafficking defects and dominant negative current suppression, respectively. A 75% loss of functional channels results in EADs.

prolongation of the APD that becomes more pronounced at slow rates. In panel B, the rate-dependent effect in an M-cell is more pronounced. At a slow CL=2000 ms, the M-cell APD is markedly prolonged and a characteristic 'shoulder-morphology' AP is observed.

When I_{Kr} is absent as a consequence of a homozygous mutation ('functional I_{Kr} knockout'), the patient phenotype is marked by severe prolongation of the QT interval and polymorphic ventricular tachyarrhythmias [15]. In Fig. 10, panels C and D, simulation of this condition results in the most severe disruption of cellular repolarization. Epicardial cells (panel A) have prolonged APD (by 29 ms at CL of 750 ms; 35 ms at a CL of 2000 ms). The 999th and 1000th beats at the indicated cycle length are shown for an M-cell in panel D. The M-cell develops EADs even at a normal human physiological cycle length of 750 ms. During severe bradycardia (CL=2000 ms) multiple EADs develop.

4. Discussion

In this study, functional defects in I_{Kr} due to several HERG mutations are introduced into a comprehensive model of the cardiac ventricular myocyte. The results demonstrate that distinct mutations can have variable effects on current morphology and lead to varying degrees of altered electrophysiology, depending on kinetic changes induced by the mutation. The use of a Markovian model to represent I_{Kr} deviates from the traditional Hodgkin–Huxely approach [34]. The Markovian scheme represents distinct channel states and coupling between these states, allowing us to relate state-specific kinetic properties of ion channels to the electrophysiological behavior of the whole cell.

Heterogeneous mutations in HERG that give rise to the same syndrome, congenital LQTS, may differ in severity

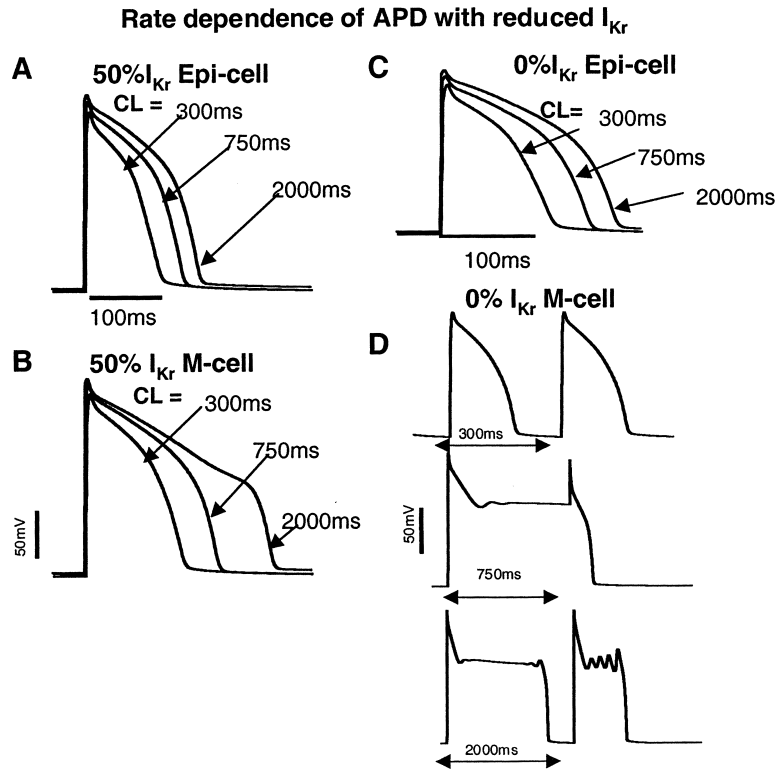

Fig. 10. The effects of a 50% reduction in I_{Kr} on APD at various cycle lengths in epicardial (A) and M-cells (B). Action potentials are from the 1000th paced beat at the indicated cycle length. The effects of a functional I_{Kr} knockout (homozygous) mutation on repolarization of the 1000th AP in epicardial (C) and the 999th and 1000th AP in M-cell (D). When I_{Kr} is absent, epicardial APDs are prolonged. M-cells develop multiple arrhythmogenic EADs at physiological (750 ms) and slow (2000 ms) CLs.

and differentially affect the morphology of I_{Kr} during the AP. The T474I mutation predominantly affects the current at the onset of the AP through a leftward shift in the voltage dependence of activation. However, recovery from inactivation and deactivation are unaffected. Hence, the morphology of the late current is preserved in the T474I mutation, as evidenced by the preservation of the pronounced peak in channel open probability (P(O)) late in cellular repolarization seen in WT cells (Fig. 6, arrow). The result is a relatively small effect on APD.

In contrast, the R56Q mutation affects deactivation kinetics that decrease I_{Kr} late in the AP. The delicate equilibrium between recovery from inactivation and deactivation is altered as a result of this defect. The increased rate of deactivation acts to 'pull' channels from the open state into closed states before they can conduct a substantial current. It is clear from examination of the current during the AP (Fig. 6, right), that late I_{Kr} is diminished due to the lack of the late maximum in channel P(O), which markedly slows AP repolarization and prolongs APD. Here, we focus on the most severe of the PAS mutations, but this behavior can be generalized to various defects that act to speed deactivation [30].

The N629D mutation gives rise to I_{Kr} that fails to inactivate. This gain of function would seemingly manifest as a larger I_{Kr} that would act to shorten APD. However, the disruption of the pore selectivity sequence that also results from the mutation allows for passage of Na^+ ions into the cell. The loss of ion selectivity gives rise to a shift in the reversal potential of I_{Kr} to -13 mV. This elevated reversal potential is crossed during the plateau repolarization phase of the action potential. Once the membrane potential falls below -13 mV, the channel passes an inward current carried by Na^+ (see Fig. 8, panel B, arrows). This inward current acts to depolarize the membrane late in the AP and prolongs APD. It results in a severe cellular phenotype similar to the effects of the ΔKPQ gain of function mutation described previously in the cardiac Na^+ channel [19]. We also investigated the effects of loss of C-type inactivation and of loss of ion selectivity individually (not shown). Loss of inactivation caused a reduction in APD due to increased I_{Kr} while loss of ion selectivity was sufficient to cause APD prolongation.

To further explore the effects of HERG mutations, we have characterized the effects of a range of reductions in G_{Kr} on the morphology of the AP. A 25, 50, or 75% reduction in current could arise in a heterozygous mutation from reduced protein expression, processing or transport defect, or from dominant negative effects, respectively [15,28,32]. A 50% reduction in I_{Kr} acts to prolong the epicardial AP slightly, but has a major prolongation effect

on the APD of M-cells especially at slow rates. A functional knockout (homozygous mutation) results in the most severe disruption of cellular repolarization, consistent with patient phenotypes observed clinically. The mutation acts to prolong APD at plateau potentials, providing sufficient time for reactivation of the L-type Ca^{2+} current, which depolarizes the cell and generates the EAD [26,31]. It should be emphasized that L-type reactivation during the prolonged plateau is common to all mutations investigated in this paper and provides the depolarizing charge during the EAD upstroke.

In general, structural and functional information is obtained from isolated membrane patches and/or cloned channels in expression systems (e.g. *Xenopus* oocytes) removed from the environment where they function physiologically. The natural cellular milieu is highly interactive and modulates single channel kinetic behavior. Cellular models are unique tools that allow for reinstitution of single channels into the cell in order to investigate integrated electrophysiological behavior. That the physiological effect of a given channel defect depends on the cellular environment is demonstrated here by the greater severity of APD prolongation and disruption of repolarization in M cells, suggesting that such mutations can increase APD differences and dispersion of repolarization in the myocardium [33]. A substrate with increased dispersion of repolarization is susceptible to the development of unidirectional conduction block and reentrant arrhythmias [2,35]. Such arrhythmias can be triggered by the EADs associated with the mutations which provide premature stimuli to a highly susceptible substrate [36].

In the context of arrhythmia, it is interesting to note that arrhythmias associated with HERG mutations and LQT2 are not rate dependent to the same extent as other forms of inherited LQTS [37]. Our simulations predict that HERG defects can lead to the development of cellular arrhythmogenic responses (APD prolongation and early afterdepolarizations) at slow rates in the absence of neural influences and may explain the development of arrhythmias in patients during sleep and relaxation. However, HERG defects have also been linked to arrhythmias in patients startled by loud noise, such as a telephone or alarm clock, suggesting a role for the autonomic nervous system in increasing susceptibility to arrhythmic events [38,39]. Previous modeling studies in our laboratory have incorporated the effects of β-adrenergic stimulation in a model of the WT cell [31]. Future efforts will expand the previous studies to investigate effects of the autonomic nervous system in the context of channelopathies including LQTS.

Acknowledgements

This work was supported by the NIH National Heart, Lung and Blood Institute grants R01-HL49054 and R37-HL33343 (to YR) and a Whitaker Foundation Development Award.

Appendix. I_{Kr} formulation

$$I_{Kr} = G_{Kr} \cdot P(O) \cdot (V_m - E_K)$$

$P(O)$ = open probability of I_{Kr}

$$G_{Kr} = 0.0135 \cdot [K^+]_{out}^{0.59}$$

$$E_K = (R \cdot T/F) \cdot \ln([K^+]_{out}/[K^+]_{in})$$

Wild-type rate constants

$C1 \rightarrow O$ or $C1 \rightarrow I$ $\quad \alpha\alpha = 65.5 \cdot 10^{-3} \cdot e^{(0.05547153 \cdot (v-36))}$

$C2 \rightarrow C1$ $\quad \alpha_{in} = 2.172$

$C3 \rightarrow C2$ $\quad \alpha = 55.5 \cdot 10^{-3} \cdot e^{(0.05547153 \cdot (v-12))}$

$C2 \rightarrow C3$ $\quad \beta = 2.357 \cdot 10^{-3} \cdot e^{(-0.036588 \cdot (v))}$

$C1 \rightarrow C2$ $\quad \beta_{in} = 1.077$

$O \rightarrow C1$ $\quad \beta\beta = 2.9357 \cdot 10^{-3} \cdot e^{(-0.02158 \cdot (v))}$

$I \rightarrow O$ $\quad \alpha i = 0.439 \cdot e^{(-0.02352 \cdot (v+25))} \cdot 4.5/[K^+]_{out}$

$O \rightarrow I$ $\quad \beta i = 0.656 \cdot e^{(0.000942 \cdot (v))} \cdot 4.5^{0.3}/[K^+]_{out}^{0.3}$

$I \rightarrow C1$ $\quad \mu = (\alpha i \cdot \beta\alpha \cdot \alpha\alpha)/(\alpha\alpha \cdot \beta i)$

T474I rates

$C1 \rightarrow O$ $\quad \alpha\alpha = 65.5 \cdot 10^{-3} \cdot e^{(0.05547153 \cdot (v+25))}$

$C3 \rightarrow C2$ $\quad \alpha = 55.5 \cdot 10^{-3} \cdot e^{(0.05547153 \cdot (v+6))}$

R56Q rates

$C2 \rightarrow C3$ $\quad \beta = 2.357 \cdot 10^{-3} \cdot e^{(-0.036588(v))} \cdot 10.5$

$O \rightarrow C1$ $\quad \beta\beta = 2.9357 \cdot 10^{-3} \cdot e^{(-0.02158 \cdot (v))} \cdot 6.3$

N629D rates

$O \rightarrow I$ $\quad \beta i = 0.0$

N629D loss of selectivity

Na:K permeability (P_{Na}/P_K) = 0.65

$$E_K = (R \cdot T/F) \cdot \ln([K^+]_{out} + P_{Na}/P_K \cdot [Na^+]_{out}/[K^+]_{in} + P_{Na}/P_K \cdot [Na^+]_{in})$$

References

[1] Keating MT, Sanguinetti MC. Molecular genetic insights into cardiovascular disease. Science 1996;272:681–685.

[2] Schwartz PJ, Priori S, Napolitano C. The Long-QT syndrome. In: Zipes DP, Jalife J, editors, Cardiac electrophysiology: from cell to bedside, 3rd ed, Philidelphia: W.B. Saunders, 2000, pp. 597–615.

[3] Roden DM, Balser JR. A plethora of mechanisms in the HERG-related long-QT syndrome: Genetics meets electrophysiology. Cardiovasc Res 1999;44:242–246.

[4] Curran ME, Splawski I, Timothy KW, Vincent GM, Green ED, Keating MT. A molecular basis for cardiac arrhythmia: HERG mutations cause long QT syndrome. Cell 1995;80:795–803.

[5] Sanguinetti MC, Jurkiewicz NK. Two components of cardiac delayed rectifier K^+ current. Differential sensitivity to block by class III antiarrhythmic agents. J Gen Physiol 1990;96:195–215.

[6] Shibasaki T. Conductance and kinetics of delayed rectifier potassium channels in nodal cells of the rabbit heart. J Physiol 1987;387:227–250.

[7] Abbott GW, Sesti F, Splawski I et al. MiRP1 forms IKr potassium channels with HERG and is associated with cardiac arrhythmia. Cell 1999;97:175–187.

[8] Petrecca K, Atanasiu R, Akhavan A, Shrier A. N-linked glycosylation sites determine HERG channel surface membrane expression. J Physiol 1999;515:41–48.

[9] Sanguinetti MC, Curran ME, Spector PS, Keating MT. Spectrum of HERG K^+ channel dysfunction in an inherited cardiac arrhythmia. Proc Natl Acad Sci USA 1996;93:2208–2212.

[10] Ficker E, Jarolimek W, Kiehn J, Baumann A, Brown AM. Molecular determinants of dofetilide block of HERG K^+ channels. Circ Res 1998;82:386–395.

[11] Smith PL, Baukrowitz T, Yellen G. The inward rectification mechanism of the HERG cardiac potassium channel. Nature 1996;379:833–836.

[12] Sanguinetti MC, Xu QP. Mutations of the S4-S linker alter activation properties of HERG potassium channels expressed in *Xenopus* oocytes. J Physiol 1999;514:667–675.

[13] Cabral JHM, Lee A, Cohen SL, Chait BT, Li M, Mackinnon R. Crystal structure and functional analysis of the HERG potassium channel N terminus: a eukaryotic PAS domain. Cell 1998;95:649–656.

[14] Lees-Miller JP, Duan Y, Teng GQ, Thorstad K, Duff HJ. Novel gain of function mechanism in K^+ channel related Long-QT Syndrome: altered gating and selectivity in the HERG1 N629D mutant. Circ Res 2000;86:507–513.

[15] Hoorntje T, Alders M, van Tintelen P et al. Homozygous premature truncation of the HERG protein: the human HERG knockout. Circulation 1999;100:1264–1267.

[16] Luo CH, Rudy Y. A dynamic model of the cardiac ventricular action potential. I. Simulations of ionic currents and concentration changes. Circ Res 1994;74:1071–1096.

[17] Zeng J, Laurita KR, Rosenbaum DS, Rudy Y. Two components of the delayed rectifier K^+ current in ventricular myocytes of the guinea pig type. Theoretical formulation and their role in repolarization. Circ Res 1995;77:140–152.

[18] Viswanathan PC, Shaw RM, Rudy Y. Effects of IKr and IKs heterogeneity on action potential duration and its rate dependence. Circulation 1999;99:2466–2474.

[19] Clancy CE, Rudy Y. Linking a genetic defect to its cellular phenotype in a cardiac arrhythmia. Nature 1999;400:566–569.

[20] Balser JR, Roden DM, Bennett PB. Global parameter optimization for cardiac potassium channel gating models. Biophys J 1990;57:433–444.

[21] Wang S, Liu S, Morales MJ, Strauss HC, Rasmusson RL. A quantitative analysis of the activation and inactivation kinetics of HERG expressed in *Xenopus* oocytes. J Physiol 1997;502:45–60.

[22] Zhou Z, Gong Q, Ye B et al. Properties of HERG channels stably expressed in HEK 293 cells studied at physiological temperature. Biophys J 1998;74:230–241.

[23] Hancox JC, Levi AJ, Witchel HJ. Time course and voltage dependence of expressed HERG current compared with the native rapid delayed rectifier K current during the cardiac ventricular action potential. Pflüger's Arch 1998;436:843–853.

[24] Kiehn J, Lacerda AE, Brown AM. Pathways of HERG inactivation. Am J Physiol 1999;277:H199–H210.

[25] Yang T, Snyders DJ, Roden DM. Rapid inactivation determines the rectification and [K+]o dependence of the rapid component of the delayed rectifier K^+ current in cardiac cells. Circ Res 1997;80:782–789.

[26] Viswanathan PC, Rudy Y. Pause induced early afterdepolarizations in the long QT syndrome: a simulation study. Cardiovasc Res 1999;42:530–542.

[27] Faber GM, Rudy Y. Action potential and contractility changes in [Na^+] overloaded cardiac myocytes: A simulation study. Biophys J 2000 (in press).

[28] Zhou Z, Gong Q, Epstein ML, January CT. HERG channel dysfunction in human long QT syndrome. Intracellular transport and functional defects. J Biol Chem 1998;273:21061–21066.

[29] Nakajima T, Furukawa T, Tanaka T et al. Novel mechanism of HERG current suppression in LQT2: shift in voltage dependence of HERG inactivation. Circ Res 1998;83:415–422.

[30] Chen J, Zou A, Splawski I, Keating MT, Sanguinetti MC. Long QT syndrome-associated mutations in the Per–Arnt–Sim (PAS) domain of HERG potassium channels accelerate channel deactivation. J Biol Chem 1999;274:10113–10118.

[31] Zeng J, Rudy Y. Early afterdepolarizations in cardiac myocytes: mechanism and rate dependence. Biophys J 1995;68:949–964.

[32] Li X, Xu J, Li M. The human delta1261 mutation of the HERG potassium channel results in a truncated protein that contains a subunit interaction domain and decreases the channel expression. J Biol Chem 1997;272:705–708.

[33] Viswanathan P, Rudy Y. Cellular arrhythmogenic effects of congenital and acquired Long-QT syndrome in the heterogeneous Myocardium. Circulation 2000;101:1192–1198.

[34] Hodgkin AL, Huxely AF. A quantitative description of membrane current and its application to conduction and excitation in nerve. J Physiol 1952;117:500–544.

[35] Antzelevitch C, Yan G, Shimuzu W, Burashnikov P. Electrical heterogeneity, the ECG, and cardiac arrhythmias. In: Zipes DP, Jalife J, editors, Cardiac electrophysiology: from cell to bedside, Philidelphia: W.B. Saunders, 2000, pp. 222–238.

[36] El-Sherif N, Chinushi M, Caref EB, Restivo M. Electrophysiological mechanism of the characteristic electrocardiographic morphology of torsade de pointes tachyarrhythmias in the long-QT syndrome: detailed analysis of ventricular tridimensional activation patterns. Circulation 1997;96:4392–4399.

[37] Schwartz PJ, Priori SG, Locati EH et al. Long QT syndrome patients with mutations of the SCN5A and HERG genes have differential responses to Na^+ channel blockade and to increases in heart rate. Implications for gene-specific therapy. Circulation 1995;92:3381–3386.

[38] Wilde AAM, Jongbloed RJE, Doevendans PA et al. Auditory stimuli as a trigger for arrhythmic events differentiate HERG-related (LQTS2) patients from KVLQT1-related patients (LQTS1). J Am Coll Cardiol 1999;33:327–332.

[39] Moss AJ, Robinson JL, Gessman L et al. Comparison of clinical and genetic variables of cardiac events associated with loud noise versus swimming among subjects with the Long QT syndrome. Am J Cardiol 1999;84:876–879.